# HAL
## archives-ouvertes.fr

# Using multi-directional high-resolution imagery from POLDER sensor to retrieve leaf area index

Ferran Gascon, Jean-Philippe Gastellu-Etchegorry, M. Leroy

## ▶ To cite this version:

**HAL Id: ird-00404930**

**http://hal.ird.fr/ird-00404930**

Submitted on 20 Jul 2009

# USING MULTI-DIRECTIONAL HIGH-RESOLUTION IMAGERY FROM POLDER SENSOR TO RETRIEVE LEAF AREA INDEX

Gascon F. (1), Gastellu-Etchegorry J.P. (2) and Leroy M. (3)

(1) ESA (European Space Agency),

TEC-EEP, Keplerlaan 1, 2200AG – Noordwijk – The Netherlands – EU

Phone: (31) 71 565 6414 – E-mail: ferran.gascon@esa.int

(2) UPS (Université Paul Sabatier),

CESBIO (Centre d'Etudes Spatiales de la BIOsphère),

18, Av. Edouard Belin, 31401 – Toulouse – France – EU

(3) CNES (Centre National d'Etudes Spatiales),

MEDIAS (MEDIterranean basin And Subtropical africa) France,

18, Av. Edouard Belin, 31401 – Toulouse – France – EU

*Corresponding author. Email: ferran.gascon@esa.int

## I. CONTEXT AND OBJECTIVES

The angular variation of land surface measurements, characterized by the BRDF (Bi-directional Reflectance Distribution Function) in the solar domain and by the BTDF (Bi-directional Temperature Distribution Function) in the thermal domain provides additional information on the structure and properties of the observed landscape (Chen *et al*., 2000; Widlowski *et al.*, 2003). Thus, for instance, multi-directional measurements are potentially useful for: (1) improving surface albedo estimates through the integration of multi-directional samples of surface BRDF (Vogt *et al.*, 2000); (2) achieving better estimates of aerosol properties and consequently obtain more accurate atmospheric corrections of remotely sensed data (Moreno, 2003); (3) retrieving the surface temperature of illuminated and shadowed areas of soil and vegetation using concurrently measurements in both solar and thermal domains (Jia *et al.*, 2003); improving the accuracy in the retrieval of biophysical variables such as leaf area index (ESA, 2001a).

Recognizing that airborne campaigns provide an efficient way to realistically simulate a collection of measurement and test the retrieval algorithms proposed for future space-borne

missions, ESA has supported three DAISEX (Digital Airborne Imaging Spectrometer Experiment) campaigns to acquire high spectral resolution data over an agricultural test-site in Spain. The goals of DAISEX, which supported the collection of multi-annual data from several airborne imaging spectrometers (Moreno, 2001), were to develop retrieval techniques for biophysical variables and to establish performance requirements for future space-borne missions. POLDER data were analysed in this study.

This research seeks to analyse the estimation of crop biophysical variables using high-resolution mono and multi-directional data. More precisely, the objective is to compare quantitatively the accuracy of a physically-based retrieval algorithms using, or not, the multidirectional features acquired by the airborne sensor POLDER (POLarization and Directionality of Earth Reflectances) (Leroy *et al*., 1997). POLDER sensor is capable of acquiring multi-spectral (with bands in the visible and near-infrared spectral regions) and multi-directional data at increments of approximately 10° in zenith angle. Retrieval involved two artificial neural networks designed to invert the 1D radiative transfer model PROSAIL (Jacquemoud *et al*., 2000; Verhoef, 1985). One neural network (A) uses as input data only the isotropic component of a BRDF (Bi-directional Reflectance Distribution Function) parametric model fitted to POLDER data. The second neural network (B) requires as input variables all components, isotropic and anisotropic, of the BRDF parametric model, thereby including anisotropic information in the retrieval process.

As PROSAIL is modelling vegetation with a relatively simple architecture and model parameters vary within large ranges, methods A and B are, in principle, applicable to any vegetative land cover, independently of its structure, as this method is ideally aimed not to be site-specific but applicable to any vegetated landscape. This is the main justification for selecting a 1D radiative transfer model, i.e. a model simulating light propagation in a horizontally homogeneous landscape. The retrieval procedures use all available directional measurements and, because of using BRDF parametric model parameters instead of using directly BRF (Bi-directional Reflectance Factor) measurements, the approach do not require the retraining of the neural network when view or illumination directions change. Thus, they are not site-specific (or crop-specific) but general approaches based on an architecturally simple radiative transfer model.

Results obtained with Methods A and B were compared in order to gauge the impact on the retrieval accuracy of a mono-directional sampling of view direction space (Method A) against that of a more extensive view direction sampling (Method B). Comparisons between

the results obtained using each method were established for *in situ* locations for which ground reference data of the Leaf Area Index (LAI) was available.

## II. SITE AND AVAILABLE DATA

The Barrax test site is a flat, 3*km* by 3*km* agricultural area centred at (39°3'N, 2°5'W) and located 28*km* from Albacete (Spain, EU) (Moreno, 2003). In order to obtain ground reference data, 4 crop types (corn, sugar beet, alfalfa and barley) were measured *in situ* at 104 locations (Figure 1). Each field sample measurement is representative of an area of around 1 $m^2$.

Figure 1

Series of airborne POLDER image data were collected at different moments of the day on June 3, 4 and 5, 1999 during the DAISEX-99 campaign (ESA, 2001b). In order to have a dense sampling of the observation directional space the study combines the data of the 3 days. The number of view directions for each ground truth location is between 51 and 62. The airborne POLDER instrument comprises nine spectral bands centred at 443, 500, 550, 590, 670, 700, 720, 800 and 864 *nm*. POLDER image data were calibrated and both geometrically and atmospherically corrected (Level 1c) by CESBIO/Noveltis (Ponchaut, 2000). The spatial resolution of the POLDER imagery, 20*m*, was degraded to 60*m* through a moving 3×3 pixel 'boxcar' average, thereby minimizing any geolocation errors between POLDER imagery and ground reference data. POLDER data at a pixel location were excluded from analysis if saturated in any band or if either a small scratch on the outer lens of POLDER or sun glint was apparent in the pixel response (Gascon *et al*., 2003). The POLDER outer lens exhibits a small scratch that is visible on some images but fortunately it falls outside the study area of many scenes. The sun glint that appears on some frames concerns viewing angles between [40°, 50°] and has roughly a 5° width over the nine spectral bands. Finally, 17 of the 104 *in situ* measurement points were discarded, as some of the new 60*m* × 60*m* pixels corresponded to locations that were deemed too close to a field border. Thus, the number of ground reference locations was reduced from 104 to 87. One of the question that rises when comparing remote sensing data with ground measurements is how compare the areas associated to each measurement. In this study the ground truth sample area is significantly smaller (of the order of 1$m^2$) than the re-sampled image pixel size (3600$m^2$). This causes a higher variability of the ground truth measurements compared to the radiometric data as is presented in Figure 2 by the NDVI (Normalized Difference Vegetation Index) (Tucker, 1979). This graph clearly shows that the variability, for a given

vegetation type, is significantly lower in the direction of the ordinate axis than in the one of the abscissa axis. Referring to Figure 2, it is also important to point out the low correlation between NDVI and LAI measurements due mainly to the presence of dry barley that has a low NDVI while having a high LAI, as the ground measured LAI includes the green and senescent fractions. This fact clearly illustrates the difficulty for retrieving LAI using a semi-empirical approach and is thus a good test site for a more sophisticated approach like the method presented in this article.

Figure 2

Comparisons between *in situ* reflectance measurements and POLDER data show an agreement within 1% relative error for two of the three soil units but up to 12% for the third unit. The larger difference is explained by the relatively small size of the soil unit compared to POLDER spatial resolution (Ponchaut, 2000). The relative noise in each band of the sensor, determined using data collected over homogeneous surfaces, was largest in the blue channels in which aerosol effects are stronger and land surface reflectance values tend to be small (Moreno, 2003). Due to these high noise levels, the blue band centred at 443nm was excluded from the following steps.

The last image pre-processing step was to fit the Li-Ross kernel-driven BRDF model, Equation 1, to the measurements of each pixel of the image (Wanner *et al.*, 1995). This model was chosen because of the good performances showed for fitting airborne POLDER data (Weiss *et al.*, 2000) with a reduced number of parameters (3).

$$LR = p1.f0 + p2.f1 + p3.f2$$
$$f0 = 1$$

$$f1 = (O(\theta_s, \theta_v, \phi) - \sec\theta_v - \sec\theta_s) + \frac{1}{2}(1 + \cos(\xi))\sec\theta_s \sec\theta_v$$

$$O(\theta_s, \theta_v, \phi) = \frac{1}{\pi}(t - \sin t.\cos t)(\sec\theta_s + \sec\theta_v)$$

$$\cos t = 2\frac{\sqrt{\Delta^2 + (\tan\theta_s \tan\theta_v \sin\phi)^2}}{\sec\theta_s + \sec\theta_v}$$

$$f2 = \frac{(\pi/2 - \xi)\cos\xi + \sin\xi}{\cos\theta_s + \cos\theta_v} - \frac{\pi}{2}$$

$$\Delta = \sqrt{\tan(\theta_s)^2 + \tan(\theta_v)^2 - (2.\tan(\theta_s).\tan(\theta_v).\sin(\phi))^2}$$

*Equation 1: Li-Ross formulation. Adjustable parameters are p1, p2 and p3. $\xi$ is the phase angle between sun and view directions. $\theta_s$ is the sun zenith angle. $\theta_v$ is the view zenith angle. $\phi$ is the azimuth angle between sun and view directions.*

The "p1" parameter corresponds to the nadir reflectance when sun zenith angle is zero. The "p2" parameter represents the bowl/bell shape of the BRDF (positive values correspond to a bell shape and negative to a bowl shape). The "p3" parameter represents the backscattering/forwardscattering shape of the BRDF (positive values are associated to a BRDF with predominant backscattering shape and negative values correspond to a BRDF with predominant forwardscattering effect).

Estimation of the fit of each of the 3 Li-Ross BRDF model parameters to the POLDER directional measurements of each 60×60*m* pixel was performed through the minimization of the error function $\varepsilon = \sum_{i=1}^{nb\_meas} \left( \rho_{simulated}(\theta_v, \theta_s, \phi) - \rho_{measured}(\theta_v, \theta_s, \phi) \right)^2$ using the quasi-Newton algorithm (Geradin *et al*., 1980). Li-Ross fitting has a RMSE (Root Mean Square Error) of 1.8% in average for all test locations and spectral bands. Figure 3 presents for one of the sugar beet test points, the fit of the Li-Ross model with the BRF measurements in the principal plane. This example, with a fitting RMSE of 1.6%, clearly illustrates the difficulty for accurately fitting the narrow hot-spot feature (linked to the inter-leaves shadowing compared to the broad hot-spot related to the canopy architecture). However, the fact of not catching this narrow feature is not a major problem, as these features will not be caught neither for the airborne nor the simulated data and consequently the retrieval will be still possible.

Figure 3

**III. RETRIEVAL ALGORITHM**

The LAI was retrieved with the aid of an artificial neural network that was trained on a lookup table (LUT) generated by the PROSAIL soil-vegetation reflectance model (Jacquemoud *et al*., 2000). PROSAIL couples three models: the SAIL canopy reflectance model (Verhoef, 1985), the PROSPECT leaf reflectance model (Jacquemoud & Baret, 1990) and SOILSPECT, a parametric soil reflectance model (Jacquemoud *et al*., 1992).

SAIL (Scattering from Arbitrarily Inclined Leaves) (Verhoef, 1985) simulates vegetation reflectance through the simulation of within vegetation radiative transfer. For that, vegetation

canopy is simulated as a homogeneous layer composed of randomly distributed leaves of infinitesimal size. Radiation interception within the vegetation cover is modelled using the Beer-Lambert law. The hot-spot phenomenon is simulated with Kuusk's approach (Kuusk, 1985) and its single parameter ("Hs"). The amount of leaves is represented by the LAI, or square meters of leaf surface per square meter of soil. Leaf orientation distribution is represented by an average leaf angle ALA (Average Leaf Angle). The model also allows one to deal simultaneously with two kinds of leaf, which is useful in this study to distinguish between green and senescent component (parameter "fsen").

PROSPECT (leaf optical PROperties SPECTra) (Jacquemoud & Baret, 1990) model simulates leaf optical properties for wavelengths from $0.4\mu m$ up to $2.4\mu m$, according to the leaf chemical composition and a structural index (N). The leaf is supposed to be a pile of N layers separated by thin air layers. If N is not an integer, for instance N=2.3, the fractional part (0.3) acts as a weight for the thickness of the third layer. For a young monocotyledonous leaf, N usually varies between 1 and 1.5. For dicotyledonous, N can reach 2.5 and even 5 for some senescent leafs (Jacquemoud, 1992). The chemical concentrations used by PROSPECT are: chlorophyll a+b $C_{ab}$ (in general $C_{ab} < 90 \mu g.cm^{-2}$), water $C_w$ (*cm*), dry matter $C_{dm}$ ($g.cm^{-2}$) and brown pigments $C_b$ ($\mu g.cm^{-2}$). The interaction of a ray with the leaf surface is simulated with the Fresnel laws (refraction index n($\lambda$)). Volume interactions are described by the Beer-Lambert law using an absorption coefficient K($\lambda$) which is a function of the chemical concentrations: $K(\lambda) = \sum_i C_i.k_i(\lambda)$ . Where $k_i(\lambda)$ is the absorption coefficient specific and $C_i$ the concentration per leaf surface unit of the biochemical component "*i*".

SOILSPECT (SOIL optical properties SPECTra) (Jacquemoud *et al*., 1992) is a parametric soil BRDF model representing reflectance with Equation 2.

$$BRF_{SOILSPECT} = \omega \cdot \left( (1+B) \cdot \left( 1 + phase1 \cdot \cos(\varphi_{xv}) + phase2 \cdot \frac{\left(3 \cdot \cos^2(\varphi_{xv}) - 1\right)}{2} \right) \right) \cdot \frac{1}{4 \cdot (\cos\theta_x + \cos\theta_v)}$$

$$\text{with} \qquad B = \frac{1}{\left(1 + h \cdot \tan(\varphi_{sv})\right)}$$

Equation 2: SOILSPECT formulation. Parameters are $\omega$, h, phase1 and phase2. $\varphi_{sv}$ is the phase angle between sun and view directions. $\varphi_{xv}$ is the phase angle between specular and view directions. $\theta_x$ is the zenith angle of the specular direction.

PROSAIL model uses input parameters shown in Table 1.

Table 1

All SOILSPECT model parameters showed a spectral variability but in order to simplify the LUT generation procedure, the structure-related parameters were considered as spectral constants (h = 1.5246, phase1=0.0155 and phase2=-1.2683) and derived for the intermediate band (670$nm$). Only albedo (w) was considered variable applying a multiplicative factor (sp) to a fixed spectral profile of reflectance values ($w_{500}$=0.551, $w_{550}$=0.637, $w_{590}$=0.717, $w_{670}$=0.770, $w_{700}$=0.786, $w_{720}$=0.796, $w_{800}$=0.825, $w_{864}$=0.840). A further modification to PROSAIL was made in the hotspot model (Kuusk, 1985) that is embedded within the SAIL model (and which is an integral part of PROSAIL); the formula for the correlation length in the hotspot model was multiplied by a correction factor ($2/(\cos(\theta_v)+\cos(\theta_s))$) in order to account for the increased shadow length associated with large zenith angles. This correction factor improves modelling results for canopies with a spherical leaf angle distribution. (Such a lengthening of shadows does not occur for canopies with horizontal leaves, which could explain why this effect has been overlooked).

The LUT was generated with input parameters that varied by constant increments between minimum and maximum values (Table 2). Total number of simulations was 524000, having between 2 and 6 sampled values for each variable. The viewing angular geometries simulated for each configuration of parameters are the combination of the zenith angles 0, 10, 20, 30, 40, 50 and 60° and the azimuth incremental angles (with respect to the principal plane) of 0, 18, 36, 54, 72, 90, 108, 126, 144, 162 and 180° which combined represent a total number of 62 directions. Only half of the directional space hemisphere is simulated, as the simulated BRFs using a 1D model are symmetrical with respect to the BRDF principal plane.

Table 2

The four soil parameters (phase1, phase2, h and ω) were derived by fitting the soil BRDF parametric model SOILSPECT to ground measurements. The multi-directional BRF ground measurements were acquired using the FIGOS (FIeld GOniometer System) instrument (Sandmeier and Itten, 1999) on the S10 bare soil parcel of the Barrax site. While all SOILSPECT model parameters did display some spectral variability, in order to simplify the LUT generation procedure, the three parameters (h, phase1 and phase2) related to structure were assumed to be constants, spectrally invariant. Only albedo (ω) was considered variable

and spectrally dependent. The specific values of phase1 and phase2 of the intermediate band (670*nm*) were applied to all bands. The fitting algorithm minimises the error function

$$\varepsilon = \sum_{i=1}^{nb\_meas} \left( BRF_{SOILSPECT}(\theta_v, \theta_x, \varphi_{xv}) - \rho_{measured}(\theta_v, \theta_x, \varphi_{xv}) \right)^2$$ using quasi-Newton method

(Geradin *et al*., 1980).

Inversion of the LUT was accomplished with the aid of a three layer perceptron, an artificial neural network architecture previously used for inverting vegetation radiative transfer models (Kimes *et al*., 2002; Weiss *et al*., 2000). The first two layers have M and O neurons and a log-sigmoid transfer function, while in the third and last layer the single output neuron has a linear transfer function (Gurney, 1997) for estimating just one variable. The algorithm pre-processes the network training set by normalizing inputs and outputs to the interval [-1,1]. Thus, every spectral band is weighted identically and independently of the range of BRF values.

Three data sets were used in the training and testing of the artificial neural network: (1) *Training data*: These are the data on which the gradient descent is performed. 70% of the input-output values were used for training. (2) *Validation data*: This dataset is not used for training. It is used to determine when the training must stop. 20% of the input-ouput values were used for validation. (3) *Test data*: This is the dataset used to assess the generalized performance of the network. 10% of the input-ouput values were used for testing.

For Method A, the inputs of the network are the 8 $p_1$ parameters of the Li-Ross model ($p_1^{500}$, $p_1^{550}$, $p_1^{590}$, $p_1^{670}$, $p_1^{700}$, $p_1^{720}$, $p_1^{800}$, $p_1^{864}$), which correspond to the nadir reflectance when the sun zenith angle is equal to 0. As said before, these parameters were derived from the fitting of the Li-Ross model with the available multi-directional measurements. For Method B, the network has 24 inputs, which correspond to the 3 Li-Ross model parameters for each of the 8 spectral bands ($p_1^{500}$, $p_2^{500}$, $p_3^{500}$, $p_1^{550}$, $p_2^{550}$, $p_3^{550}$, etc.). A specific neural network was defined for each of the retrieved variables. When defining neural network architecture, it must be taken into account that an overly simplified architecture does not reproduce accurately the non-linearity of the inverse radiative transfer function, which tends to lead to inaccurate results. Conversely, an overly complex network provides a perfect fitting of the training samples but a more erroneous estimation of values away from the training data. Hence, the sizing of the neural network is driven by this trade-off. In this study, to solve this issue the architectural parameters, i.e. M and O, were defined by minimizing the RMSE between estimated and ground-measured parameters.

## IV. RESULTS

To analyse the quality of the results obtained using the two retrieval methods, we identified five possible sources of error: (a) erroneous or inaccurate remote sensing data; (b) inaccurate ground measurements; (c) spatial mismatch between airborne and field measurements; (d) an erroneous or inaccurate retrieval algorithm; and (e) inaccurate or not realistic BRF physical modelling. Sources (a) and (e) are analysed in this study with the aid of histograms of the Li-Ross model parameters ($p_1$, $p_2$, $p_3$) (Figure 4). The domain of each histogram was divided into 20 bins. The shape of each histogram of the measurements aided identification of artefacts or a poor fit between simulations and measurements.

Figure 4

For Method A, the neural network architecture was defined by M=4 and O=4, using the strategy described previously at the end of chapter III. The network was trained with 35 epochs (or iterations). LAI coefficient of determination using the training data is $r^2$=89%. Estimated and *in situ* measurements have a coefficient of determination of 68% (Figure 5). This coefficient is larger than the 44% obtained using a semi-empirical method based on NDVI (Figure 2). The RMSE between measured and *in situ* measurements is 0.87 (Table 3). Sugar and corn have a low RMSE (0.5). In the case of the corn, a crop with low LAI, retrieval algorithm corrects the strong soil component of the radiometric measurements. For "barley" the RMSE is higher (1.22) and retrieval slightly underestimates LAI compared to ground measurements. "Alfalfa" leads to larger RMSE (1.36) with LAI overestimated. These results clearly show the advantage of using a physically-based method compared to the use of a NDVI-based semi-empirical approach (Figure 2). This is clearly illustrated by the fact that "corn" and "barley" have similar NDVI levels while having significantly different LAI. Thus this advantage is not only in terms of adaptability, i.e. use of the algorithm in other experimental conditions, but also in terms of accuracy of the estimates. A final remark is that this mono-directional retrieval algorithm was not employed in the case of high LAI values (i.e. higher than 4) in which case, generally, retrieval methods have more difficulties in accurately retrieving LAI.

Figure 5

Table 3

For Method B, the neural network architecture is defined by M=6 and O=3, and was trained with 25 epochs (or iterations). LAI coefficient of determination using the training data is

$r^2=94\%$, i.e. this is the theoretically better performance of the retrieval algorithm. Although this coefficient is larger than using Method A, estimated and *in situ* LAI measurements are less well correlated than method A (52%) when is tested using real measurements. Furthermore, RMSE is larger (3.29) than using Method A (0.87). For each crop type, LAI values are overestimated (Figure 7) and RMSE is always larger than those obtained with Method A (Table 4). To understand this degradation of the results when using multidirectional information, the histograms of the Li-Ross parameters "p1", "p2" and "p3" were analysed.

For "alfalfa", "sugar" and "corn", measured "p3" parameters for the visible band centred at 500*nm* have larger values than the mean of PROSAIL simulated "p3" values (Figure 4). For "barley" this phenomenon is also present but less accentuated, which translates into a more accurate retrieval compared to other crops. For the near infrared band at 864*nm* measured "p3" values are close to the means of PROSAIL simulated values. However, there is still incoherence between measured and simulated BRF values. In the example of Figure 6, we state that the p3 parameter is clearly divergent, being 0.47 for the measurements and 0.31 in averages for the simulations with LAI within the range defined by the ground measured LAI value plus/minus 1. Hence, we can conclude that modelled and measured data are not coherent for the backscattering component of the reflectance and this degrades the retrieval using the anisotropic parameter "p3".

Figure 6

Figure 7

Table 4

## V. CONCLUDING REMARKS

The goal of this study was to analyse the performance of a biophysical variables retrieval algorithm using mono-directional or multi-directional airborne multi-spectral measurements. The retrieval algorithm is based on inverting a 1D soil-vegetation radiative transfer model (PROSAIL) using a neural network. Retrieval method shows good performance for retrieving LAI when using mono-directional data. The coefficient of determination is 68% and RMSE is 0.87. Compared with classical regression techniques, the physically based approach significantly improves the accuracy of the estimates. However, these results are not improved when using multi-directional data. In this case, the coefficient of determination is lower (52%) and RMSE is significantly larger (3.2). These results are deceiving when

compared to the theoretical improvement that is expected when using simulated data. The study showed that one of the main sources of error is the incoherence between POLDER sensor measurements and model-simulated BRFs (Figure 6). Measurements of p3 outside the range of the training values of the neural network induce large estimation errors. Atmospheric correction could be an additional source of error, as the atmospheric corrections were made assuming a simple BRDF lambertian model for the target reflectance and considering an identical BRDF for neighbouring pixels. The significant degradation of the results when using multi-directional data can also be due to the used retrieval algorithm which offers good performance when p1 measurements match but completely erroneous when p3 (i.e. multidirectional information) is putted in play.

Three recommendations are proposed for improving this situation:

- Improve the modelling of soil-vegetation radiative transfer, if necessary going from 1D to 3D architectures, to more accurately reproduce the BRDF of different crop types. In particular, backscattering (which is linked to architectural features of the crop) should be improved, as strong mismatches between simulations and measurements were reported. A detailed comparison between 1D and 3D modelling is described in (Gascon, 2005).

- When using multi-directional data, apply more accurate atmospheric correction algorithms, which take into account the anisotropy of the ground target and the heterogeneity of the surrounding area.

- When using neural networks, ensure that the network is trained for all possible input combinations. Otherwise, an input outside the range of the training values will produce aberrant output results.

Finally, point out that the results obtained in this study have been compared to those obtained by two other teams from INRA (Institut National de la Recherche Agronomique) and the UV (Universitat de València) (García-Haro *et al*., 2004) and results will be published as well (Gascon *et al*., 2005).

1
2
3
4
5
6
7
8
9
10
11
12
13
14
15
16
17
18
19
20
21
22
23
24
25
26
27
28
29
30
31
32
33
34
35
36
37
38
39
40
41
42
43
44
45
46
47
48
49
50
51
52
53
54
55
56
57
58
59
60

For Peer Review Only

**References:**

Chen, J., Li, X., Nilson, T., & Strahler, A. (2000). Recent advances in geometric-optical modeling and its applications, Remote Sensing Review, 18, 227-262.

ESA (European Space Agency) (2001a). SPECTRA – Surface Processes and Ecosystem Changes Through Response Analysis. ESA SP-1257 (5).

ESA (European Space Agency) (2001b). DAISEX (Digital AIrborne Spectrometer EXperiment. ESA SP-499.

García-Haro, F.J., Camacho-de Coca, F., & Meliá, J., (2004). 'DISMA - A directional Spectral Mixture Analysis Method. Application to multi-angular airborne measurements'. Submitted to International Journal of Remote Sensing.

Gascon, F., Gastellu-Etchegorry, J.P., & Leroy, M. (2003). Scientific Analysis of the ESA Airborne Multi-Annual Imaging Spectrometer Campaign DAISEX. Final report of the 24th of April 2003, CESBIO, Toulouse, France.

Gascon, F., Bacour, C., Camacho-de Coca, F., García-Haro, J. (2004). Comparison of physically based methods for retrieving leaf area index during the DAISEX study. Submitted to Remote Sensing of Environment.

Gascon, 2005. Comparison of 1D and 3D radiative transfer modelling for simulating pine forest BRF measurements. Submitted to IEEE Transactions on Geoscience and Remote Sensing.

Geradin, M., Idelsohn, S.R., & Hogge, M. (1980). Computational Strategies for the Solution of Large Nonlinear Problems via Quasi-Newton Methods". Computer and Structures, Published by Pergamon Press Ltd. , Vol. 13, pp. 73-81.

Gurney, K., (1997). An introduction to neural networks. UCL Press, ISBN: 1857285034.

Jacquemoud, S., & Baret, F., (1990). PROSPECT : A model of leaf optical properties spectra, Remote Sensing of Environment, 34 :75-91.

Jacquemoud, S., Bacour, C., Poilvé, H. & Frangi, J.-P. (2000). Comparison of Four Radiative Transfer Models to Simulate Plant Canopies Reflectance: Direct and Inverse Mode. Remote Sensing of Environment, 74, 471-481

Jacquemoud, S., Baret, F., & Hanocq, J. (1992). Modeling spectral and directional soil reflectance, Remote Sens. Environ., 41:123-132.

Jia, L., Li, Z.-L., Menenti, M., Su, Z., Verhoef, W., & Wan, Z., (2003), A practical algorithm to infer soil and foliage component temperatures from bi-angular ATSR-2 data. International Journal of Remote Sensing. In press.

Kimes, D., Gastellu-Etchegorry, J.P., & Estève, P. (2002). Recovery of forest canopy haracteristics through inversion of a complex 3D model, Remote Sensing of the Environment, 79: 320-328.

Kuusk, A., (1985). The hot spot effect of a uniform vegetative cover, Soviet Journal of Remote Sensing, 3, 645-658.

Leroy, M., Deuze, J.L., Bréon, F.M., Hautecoeur, O., Herman, M., Buriez, J.C., Tanre, D., Bouffies, S., Chazette, P., & Roujean, J.L. (1997). Retrieval of atmospheric properties and surface bidirectional reflectances over the land from POLDER. Journal of Geophycal Research., vol 102, #D14, pp17023-17037.

Moreno, J. F. (2001). Scientific Analysis of the ESA Airborne Multi-Annual Imaging Spectrometer Campaign DAISEX. Proposal UVAL-2001/01 27/03/2001 in response to Invitation to Tender AO/1-3805/00/NL/MM of the European Space Agency.

Moreno, J. F. (2003). Scientific Analysis of the ESA Airborne Multi-Annual Imaging Spectrometer Campaign DAISEX. Final report of the study AO/1-3805/00/NL/MM of the European Space Agency.

Ponchaut, F. (2000). Processing of the POLDER Airborne data set acquired during the DAISEX "99 campaign. Final report of the 21$^{st}$ of February 2000, Noveltis Company, Toulouse, France.

Sandmeier, S., & Itten, K.I. (1999). A Field Goniometer System (FIGOS) for Acquisition of Hyperspectral BRDF Data. IEEE Transactions on Geoscience and Remote Sensing, 37(2), 978-986.

Tucker, C.J. (1979). Red and photographic infrared linear combinations for monitoring vegetation. Remote Sensing of the Environment, 8, 127-150.

Verhoef, W. (1985). Earth observation modeling based on layer scattering matrices. Remote Sensing of Environment, 17, 164-178.

Vogt, P., M., Verstraete, M., Pinty, B., Menenti, M., Caramagno, A., Rast, M., and Lajas D. (2000). The Impact of Multi-angular Measurements on the Accuracy of Land-Surface Albedo Retrieval: Preliminary Results for the Proposed ESA LSPIM Mission. Remote Sensing Reviews, 19, 191-204.

Wanner, W., Li, X., & Strahler, A.H. (1995). On the derivation of kernel-driven models of bidirectional reflectance. Journal of Geophysical Research, 100, D 10, 21077-21089.

Weiss, M., Jacob, F., Baret, F., Pragnère, A., Bruchou, C., Leroy, M., Hautecoeur, O., Prévot, L., Bruguier, N. (2002). Evaluation of kernel-driven BRDF models for the normalization of Alpilles/ReSeDA POLDER data. Agronomie (France) Special Issue. Vol. 22 no. 6; 531-536.

Weiss, M., Baret, F., Leroy, M., Hautecoeur, O., Prévot, L., & Bruguier, N. (2000). Validation of Neural Network Techniques for the Estimation of Canopy Biophysical Variables from Vegetation data. Agronomie, 20, 3-22.

Widlowski, J.-L., Pinty, B., Gobron, N., Verstraete, M. M., Diner, D. J., & Davis, A. B. (2003). Towards Land Structure Parameters from Multi-angular Remote Sensing Data. *Climatic Change*, in print.

1
2
3
4
5
6
7
8
9
10
11
12
13
14
15
16
17
18
19
20
21
22
23
24
25
26
27
28
29
30
31
32
33
34
35
36
37
38
39
40
41
42
43
44
45
46
47
48
49
50
51
52
53
54
55
56
57
58
59
60
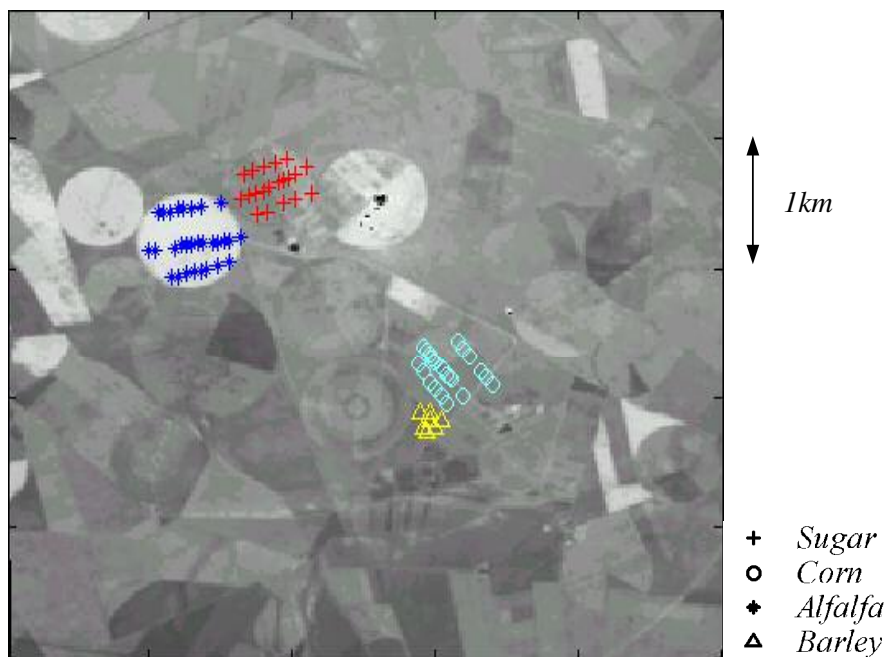
For Peer Review Only

16

Figures



Figure 1: Location of the *in situ* measurement points on a POLDER image (band centred at 550 *nm*). The image is centred at (39°3'N, 2°5'W).
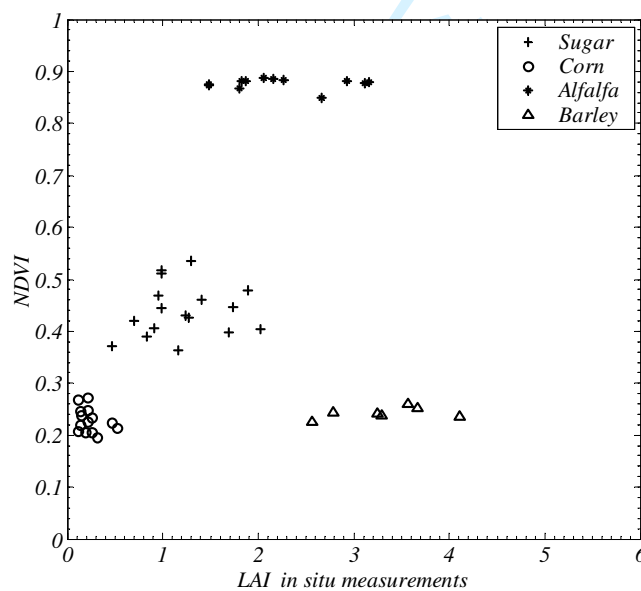


Figure 2: Comparison between NDVI (Normalized Differential Vegetation Index) and *in situ* data.
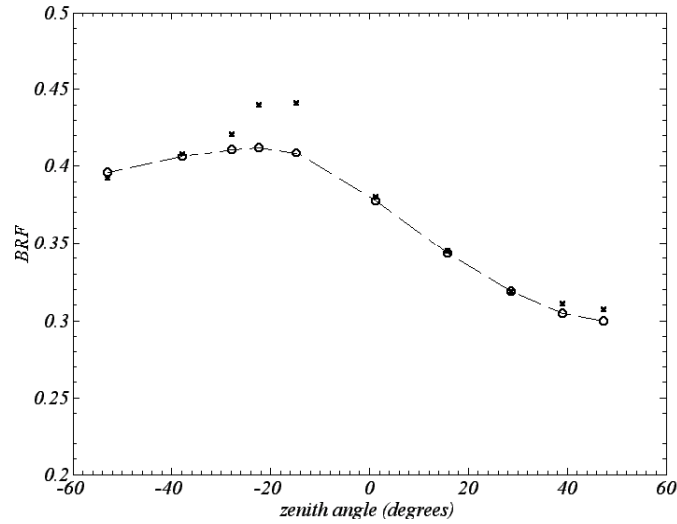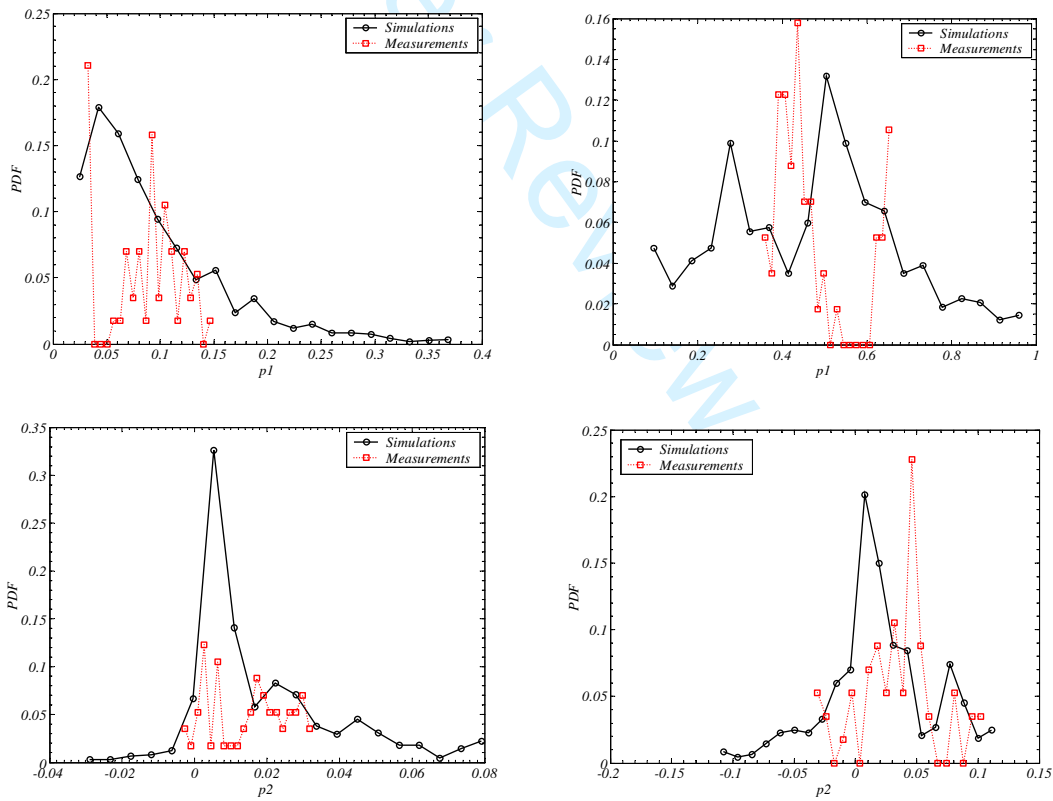
Figure 3: Comparison of the BRF values (band 864$nm$) in the principal plane for a sugar beet sample point (UTME = 577647$m$, UTMN = 4324723$m$). The RMSE between measured BRF values (x) and Li-Ross model values (o) is 1.6%.
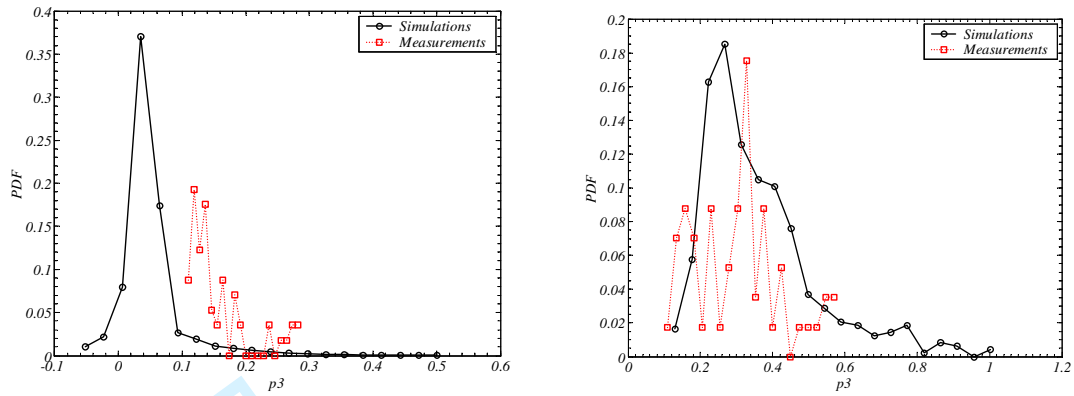
Figure 4: Histograms of simulated and measured Li-Ross parameters p1 (upper histograms), p2 (middle histograms) and p3 (lower histograms). Bands cantered at 500 *nm* (left) and 864 *nm* (right). PDF (Probability Distribution Function) = number of counts/total number of counts considering 20 sampling intervals. Simulated data used for generating the histograms correspond to the whole dataset used for the training of the neural network and measurements correspond to the radiometric data associated to the test locations.
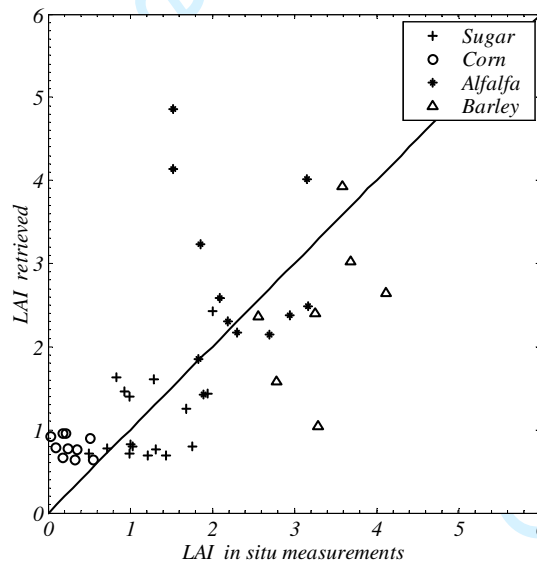


Figure 5: Comparison between retrieved values and *in situ* measurements using Method A.
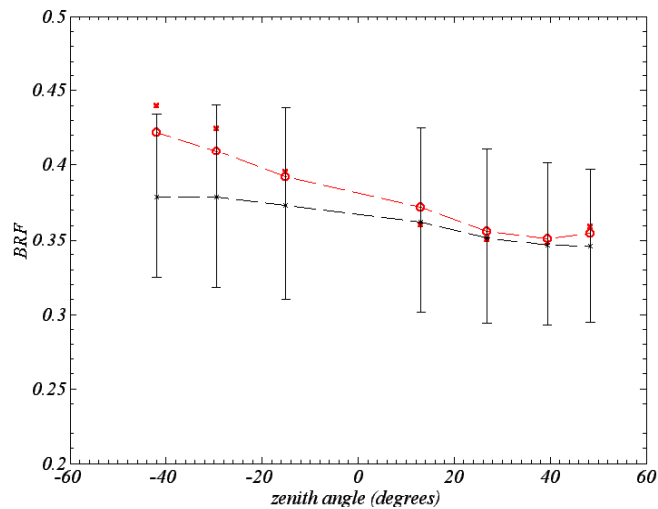
Figure 6: Comparison of the BRF values (band 864*nm*) within an acquisition track over a barley test location (UTME = 579037*m*, UTMN = 4322827*m*, LAI measured *in situ* = 4.2 ). Measured BRF values (x) are fitted with the Li-Ross model (o) and compared to PROSAIL simulations (*) with their associated range when varying LAI between 3.2 and 5.2 .
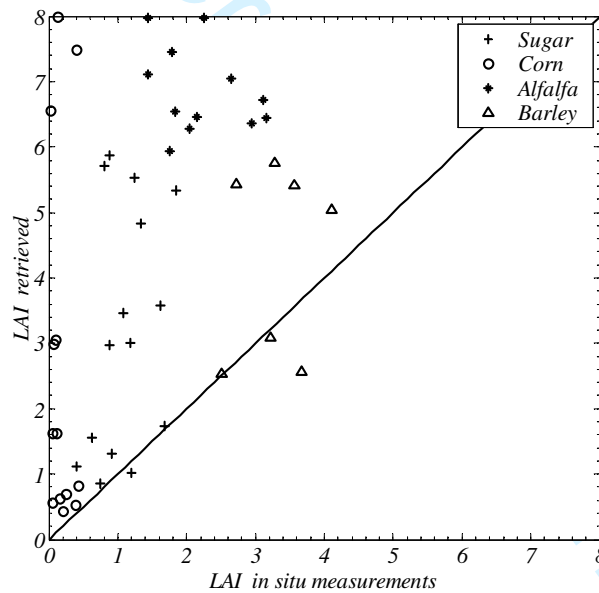


Figure 7: LAI retrieved values and *in situ* measurements using Method B.

Tables

| | Abbreviation | Parameter Name | Unit |
|---|---|---|---|
| **Green leafs properties** | $N_g$ | Structure index | no unit |
| | $C_{ab,g}$ | Chlorophyll concentration | $\mu gr.cm^{-2}$ |
| | $C_{dmg}$ | Dry mater content | $gr.cm^{-2}$ |
| | $C_{w,g}$ | Water content | $cm^{-1}$ |
| | $C_{b,g}$ | Brown pigments content | $\mu gr.cm^{-2}$ |
| **Senescent leafs properties** | $N_s$ | Structure index | no unit |
| | $C_{ab,s}$ | Chlorophyll concentration | $\mu gr.cm^{-2}$ |
| | $C_{dm,s}$ | Dry mater content | $gr.cm^{-2}$ |
| | $C_{w,s}$ | Water thickness | $cm^{-1}$ |
| | $C_{b,s}$ | Brown pigments content | $\mu gr.cm^{-2}$ |
| **Canopy Structure** | LAI | Leaf Area Index | no unit |
| | fsen | Fraction of senescent vegetation | % |
| | ALA | Average Leaf Angle | ° |
| | Hs | Hot spot parameter | no unit |
| **Soil BRDF** | sp | Soil albedo factor | no unit |
| | ω | SOILSPECT albedo | no unit |
| | phase1 | SOILSPECT parameter phase1 | no unit |
| | phase2 | SOILSPECT parameter phase2 | no unit |
| | h | SOILSPECT hot spot parameter | no unit |
| **Angular geometry** | θs | Sun zenith angle | ° |
| | Δφ | Delta between sun and view azimuth angles | ° |
| | θv | View zenith angle | ° |

Table 1: Input parameters of the PROSAIL model.

| Parameter | Min. value | Max. value |
|---|---|---|
| $N_g$ | 1 | 2.5 |
| $C_{ab,g}$ | 5 | 70 |
| $C_{dmg}$ | 0.002 | 0.02 |
| $C_{b,g}$ | 0 | 3 |
| $N_s$ | 1.5 | 3 |
| $C_{ab,s}$ | 0 | 0 |
| $C_{dm,s}$ | 0.002 | 0.02 |
| $C_{b,s}$ | 0 | 3 |
| LAI | 0 | 8 |
| fsen | 0 | 1 |
| ALA | 35 | 80 |
| Hs | 0.01 | 0.5 |
| sp | 0.25 | 1.5 |

Table 2: Variation range of input parameters of the PROSAIL model used to generate the training LUT.

| Crop | RMSE |
|---|---|
| Sugar | 0.50 |
| Corn | 0.52 |

| | |
|---|---|
| Alfalfa | 1.36 |
| Barley | 1.22 |
| **Total** | 0.87 |

Table 3: RMSE between LAI retrieved values and *in situ* measurements using Method A.

| **Crop** | **RMSE** |
|---|---|
| Sugar | 2.98 |
| Corn | 2.95 |
| Alfalfa | 4.70 |
| Barley | 1.63 |
| **Total** | 3.29 |

Table 4: RMSE between LAI retrieved values and *in situ* measurements using Method B.